Journal of Geophysical Research: Space Physics

RESEARCH ARTICLE
10.1029/2018JA025798

Key Points:
- Large *F* region zonal plasma drifts are observed 20 min prior to the earthquake at 2,200 km away from epicenter
- Earthquake-linked strong vertical downward electric field of 3 mV/m is present in the *F* region on 28 March 2005
- Tsunami- and earthquake-linked effects on *F* region zonal plasma drifts persist even 18.5 hr after the earthquake on 26 December 2004

Correspondence to:
P. Gurram,
padmagurram123@gmail.com

Citation:
Gurram, P., Kakad, B., Ravi Kumar, M., & Bhattacharyya, A. (2019). Earthquake/tsunami-linked imprints in the equatorial *F* region zonal plasma drifts and spatial structures of plasma bubbles. *Journal of Geophysical Research: Space Physics*, *124*, 504–520. https://doi.org/10.1029/2018JA025798

Received 19 JUN 2018
Accepted 22 NOV 2018
Accepted article online 10 DEC 2018
Published online 5 JAN 2019

Earthquake/Tsunami-Linked Imprints in the Equatorial *F* Region Zonal Plasma Drifts and Spatial Structures of Plasma Bubbles

P. Gurram[1], B. Kakad[1,2], M. Ravi Kumar[1], and A. Bhattacharyya[1]

[1]Indian Institute of Geomagnetism, Navi Mumbai, India, [2]Research Institute for Sustainable Humanosphere, Kyoto University, Japan

Abstract We report preseismic and postseismic distinct features observed in equatorial ionospheric *F* region in Indian longitude during two major earthquakes that occurred on 28 March 2005 (M_w = 8.6) and 26 December 2004 (M_w = 9.1) with epicenters near Sumatra, Indonesia. We used spaced receiver scintillation observations on a 251-MHz signal transmitted from a geostationary satellite and recorded at dip equatorial station Tirunelveli, which is ≈2,200 km away from the epicenter of these earthquakes. On 28 March 2005, we noticed significant enhancement (≈88.5 m/s) in *F* region zonal plasma drift as compared to their seasonal quiet time drifts, 20 min prior to the start of earthquake. This implies the presence of additional vertically downward electric field of approximately 3 mV/m, which is linked with the earthquake mechanism. It is unusual because so far we have not encountered such feature on either magnetically quiet or disturbed days. Spatial scales associated with equatorial spread *F* irregularities generated in the postsunset hours on this earthquake day are considerably smaller. It suggests that the earthquake-linked electric field influenced the structuring and evolution of equatorial spread *F* irregularities on this earthquake day. Another earthquake that occurred on 26 December 2004 triggered a tsunami. We noticed that the earthquake- and tsunami-linked effects in the *F* region plasma drifts are distinctly observed even 18.5 hr after the earthquake.

1. Introduction

Ionospheric plasma is influenced by the forcing from above and the forcing from below. Forcing from above mainly includes the effect of electromagnetic radiations and the energetic particles emitted from the sun, which modifies the ionospheric plasma via ionization processes, thermal interactions, and electric fields. It also affects the ambient dynamo electric fields generated at ionospheric altitude by neutral winds under the influence of pressure gradient forces. On the other hand, forcing from below includes the effects through tides, winds, and waves in the lower thermosphere. Sometimes the disturbance associated with the lithosphere mainly due to volcanic eruptions, earthquakes, and human activity like nuclear explosions are observed in the ionosphere (Baker & Davies, 1968; Dieminger & Kohl, 1962; Gupta & Upadhayaya, 2017; Occhipinti et al., 2018; Rozhnoi et al., 2014; Shults et al., 2016). These phenomena are also considered as the potential sources for forcing from below. Earthquakes are most severe natural phenomena that have huge diverse impact on our life and infrastructure (Doocy et al., 2013; Ghobarah et al., 2006). It has been the aim of many projects to develop a forecasting model for earthquakes based on all available precursor information (Geller, 1997; Jordan & Jones, 2010; Rhoades & Evison, 2005; Wyss, 1997). However, development of such a model is not a straightforward task and it involves the meticulous study of multipoint, multi-instrument long-term observations in seismically active regions. Also, one has to be extremely cautious in treating particular observation as a precursor and check consistency in their occurrence prior to different earthquakes. So far, there has not been any success toward providing such a forecasting model. However, it is important to gather and report preseismic, coseismic, and postseismic observations in the near-Earth environment to improve our understanding of this catastrophic phenomenon.

Earthquakes occur due to Earth's lithospheric plate movement, which suddenly releases energy into the atmosphere. These energies are in the form of acoustic waves, electromagnetic waves, thermal energies, and electric fields; their signatures are observed on the ground, lower atmosphere, ionosphere, and magnetosphere, and they can be preseismic, coseismic, and postseismic (Currie & Waters, 2014; Ouzounov et al., 2018;

Reddy et al., 2015; Zhang et al., 2012). Pulinets and Ouzounov (2011) have suggested that the preseismic ionospheric disturbances can be treated as precursors for the earthquake. Generally, the anomalous distinct effects observed before and after the earthquake are respectively termed as preseismic and postseismic effects, whereas the coseismic effects are seen during the earthquake. From the geophysical point of view, the duration of an earthquake is decided by the time taken for fault rupture and the time for which shaking is felt. The earthquake durations vary from few seconds to few minutes depending upon the nature and magnitude of the earthquake. For the earthquakes considered in the present study, namely, 28 March 20005 and 26 December 2004, the earthquake durations are 120 and 480 s, respectively (Ishii et al., 2005; Walker et al., 2005). The disturbances caused by acoustic gravity waves generated by ground displacement at the time of the earthquake generally takes some time to reach the ionosphere (approximately few minutes to tens of minutes). This is because the typical speed of acoustic waves in the Earth's atmosphere (<300 km) is in the range of 240–700 m/s (Ma, 2016). So such effects shall be treated as the postseismic effects. However, it is noted that in some studies these effects have been considered as coseismic (Cahyadi & Heki, 2013; Rolland et al., 2011) and it could be because their signatures are manifested immediately after the earthquake.

During large-intensity earthquakes ($M_w > 5$), the ionospheric variations related with seismic activity can be observed few days or few hours before the arrival of the main shock of earthquakes (Liu et al., 2000; Pulinets, 1998; Silina et al., 2001). Studies have reported preseismic (Dautermann et al., 2007; Heki & Enomoto, 2013; Liu et al., 2004), coseismic (Astafyeva et al., 2014), and postseismic (Garcia et al., 2005; Marchand & Berthelier, 2008) ionospheric disturbances, and they have proposed possible physical mechanisms to explain these ionospheric imprints. So far, two mechanisms are in place to explain the seismic-ionospheric coupling. In the first mechanism, the atmospheric acoustic gravity waves are excited by the vertical ground displacement or underground gas release during earthquake preparation time, which propagate to the ionosphere affecting the ionization (Garmash et al., 1989; Harrison et al., 2010; Kim & Nikiforova, 1997; Pulinets & Davidenko, 2014; Rolland et al., 2011; Shalimov & Gokhberg, 1998; Zhou et al., 2017). In the second mechanism, an additional vertical electric field penetrates into the ionosphere due to earthquake fault rupture, which causes redistribution of charged particles (Freund, 2000; Hadjicontis & Mavromatou, 1996; Hao, 1988; Pulinets, 2009). Kim et al. (2012) have estimated the strength of seismic origin electric field penetrating into the ionosphere within the earthquake preparation zone. For these theoretical calculations they solved the Laplace's equation satisfied by the electrostatic potential with appropriate boundary conditions at the ionosphere, where divergence-free currents ($\nabla \cdot \vec{J} = 0$) are assumed to flow. These electric fields can be seen few days prior to the earthquake (Pulinets & Boyarchuk, 2004), and they can influence the ambient electric field and hence the electron plasma density few days before an earthquake.

Besides there are studies that report earthquake-linked signatures in the low-latitude ionosphere (Bhattacharya et al., 2009; Depueva, 2012; Oyama et al., 2008). The dynamics of equatorial ionosphere is different as compared to midlatitude and high-latitude ionosphere, because the Earth's magnetic field is nearly horizontal at the dip equator. This horizontal magnetic field in the presence of electric field gives rise to peculiar phenomena like equatorial electrojet, equatorial ionization anomaly, prereversal enhancement, and equatorial spread *F* (ESF) irregularities (Kelley, 2009; Lin et al., 2007; Reddy, 1989). Occurrence of ESF irregularities is a nighttime phenomenon, which is generated through nonlinear evolution of Rayleigh-Taylor (RT) plasma instability in the equatorial ionospheric *F* region during postsunset hours. The *F* layer is raised to higher altitudes due to enhanced eastward electric field through $\vec{E} \times \vec{B}$ drifts, and this lift-up plays an important role in setting up the favorable conditions for the initiation of RT plasma instability (Kelley et al., 1982). Pulinets (2009) reported the possibility of anomalous seismogenic zonal electric field generation in the earthquake preparatory zone, which can result in increased vertical plasma drifts as compared to the quiet days. Because of this increased vertical plasma drifts, the *F* layer is raised to the higher altitude, where the occurrence of RT plasma instability is more likely. Kuo et al. (2011) have suggested that observations of nighttime plasma bubble and total electron content (TEC) variations in the earthquake preparatory zone can be used as precursors for earthquake prediction. Pulinets (2012) have reported that in the low latitudes the generation of plasma bubbles is more likely before the earthquake. Few studies have explored the link between ESF irregularities and earthquakes. In our study, we report the difference in the structuring of ESF irregularities generated on the earthquake day as compared to that on other quiet days of that season, and it is attributed to the earthquake-linked electric field. As yet this aspect is not reported in earlier studies.

We are reporting preseismic and postseismic signatures of earthquakes in the equatorial *F* region during two major earthquakes that occurred on 26 December 2004 ($M_w = 9.1$) and 28 March 2005 ($M_w = 8.6$) with

epicenters near Sumatra region, Indonesia. Spaced receiver scintillation observations at dip equatorial station, which is nearly 2,200 km away from the epicenter, are used in the present study. Data used and analysis technique are described in section 2. The details of the earthquakes under study are given in section 3. The peculiar observation in the equatorial ionospheric *F* region during the earthquake time is described in section 4. The present work is discussed in section 5, and it is summarized and concluded in section 6.

2. Data and Analysis Technique

We have used amplitude scintillation observations on a 251-MHz signal transmitted from the geostationary satellite UFO2 (71.2°E) and recorded by two spaced receivers aligned in magnetic east-west direction at Tirunelveli (8.7°N, 77.8°E, dip latitude 1.5°N). The sampling interval is 0.1 s, and the receivers are separated by a distance of $x_0 = 540$ m. The amplitude scintillations during March 2005 and December 2004 are utilized in the present study as it includes the observations during two major earthquakes that occurred on (i) 28 March 2005 and (ii) 26 December 2004. In addition, the amplitude scintillation observations during April 2005, November 2004, and February 2005 are utilized to get the quiet time trends of the estimated parameters for corresponding seasons. Overall, we have 11, 2, 1, 6, and 8 quiet days with scintillations during March 2005, April 2005, November 2004, December 2004, and February 2005, respectively. We could not use observations of January 2005 as the experiment was not running during this month. It may be noted that 2004 and 2005 fall into low solar activity period, and therefore less scintillation occurrence is observed.

Spaced receiver scintillation technique has been used to study the dynamics of low-latitude ionospheric irregularities (Bhattacharyya et al., 1989; Engavale et al., 2005; Valladares et al., 1996). Meaningful information about ESF irregularities can be obtained from these spaced receiver scintillation observations by applying full cross-correlation technique introduced by Briggs (1984). In this technique the space-time correlation function of intensity variations recorded by spaced receivers is assumed to have the following form

$$C_I(x,t) = f((x - V_0 t)^2 + V_c^2 t^2) \tag{1}$$

Here f is a monotonically decreasing function of its argument $S = [(x - V_0 t)^2 + V_c^2 t^2]$ such that it has maximum value of 1 at $S = 0$. Here V_0 is the average drift speed of scintillation pattern along the base line in the receiver's plane and V_c is random velocity, a measure of random changes in the irregularity characteristics. Computation of V_0 and V_C from spaced receiver observations does not require information about the form of the cross-correlation function f (Spatz et al., 1988). By estimating the time t_m of maximum cross correlation (i.e., $C_I(x_0,t)|_{\max} = C_I(x_0,t_m)$), and time t_p, where autocorrelation function of intensity variations has the same value as maximum cross correlation (i.e., $C_I(0,t_p) = C_I(x_0,t_m)$), one can compute parameters V_0 and V_c using $V_0 = x_0 t_m/(t_m^2 + t_p^2)$ and $V_c = x_0 t_p/(t_m^2 + t_p^2)$. As receivers are separated by fixed distance, here we take $x = x_0$. So we estimated parameters, S_4, $C_I(x_0,t_m)$, V_0, and V_c for every 180 s. S_4 index is defined as the standard deviation of the normalized intensity variations, and it gives strength of the scintillations. $C_I(x_0,t_m)$ is the maximum cross correlation between intensity variations recorded by the two receivers. V_0 and V_C are estimated only when $C_I(x_0,t_m) \geq 0.5$, as the assumed dependence of f on x and t is valid at $t = t_p$ only if the decorrelation of signals from two receivers is not too large. Similarly, this technique is applied to retrieve meaningful information only if the scintillations are well above the noise level, that is, $S_4 \geq 0.15$. We have also computed coherence scale d_I defined as the 50% decorrelation scale length, that is, $C_I(x = d_I, t = 0) = 0.5$. It represents the dominant spatial scale present in the ground scintillation pattern. It should be noted that the knowledge of the exact form of function f is essential to get the coherence scale. Bhattacharyya et al. (2003) introduced a method to get the coherence scale by plotting $C_I(x_0,t_m)$ versus $x_0 V_c/(V_0^2 + V_c^2)^{1/2}$. By using the expression of t_m in $C_I(x_0,t_m)$ it is seen that such a plot represents a plot of spatial correlation function $C_I(x,0)$). This method is applied to scintillation data, and its seasonal and solar flux dependence is studied by Engavale et al. (2005). It may be noted that the distance between the receivers x_0 is generally of the order of Fresnel scale $d_F = \sqrt{2\lambda Z}$, where λ is the wavelength of the incoming radio wave, and Z is the height of irregularity layer (Kakad, Nayak, & Bhattacharyya, 2012; Yeh & Liu, 1982). For a signal of 251 MHz, traversing through ESF irregularity layer situated at the altitudes of 250–550 km, the Fresnel scale comes out to be 800–1,100 m. Although x_0 is used in the calculation of the functional form of $f(x^2)$ as discussed above, the results for the functional form of f do not depend on x_0. The functional form of f gives the spatial correlation function, which is used to determine the coherence scale d_I. Thus, the estimated values of spatial scales are not affected by the choice of x_0.

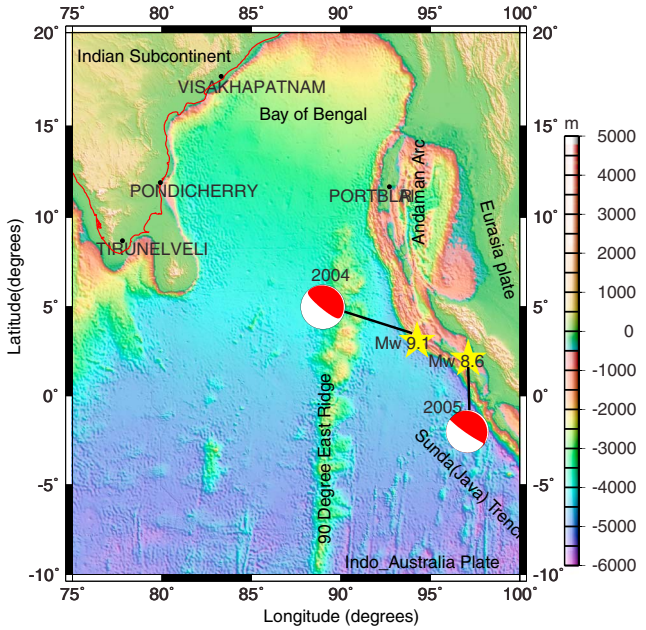

Figure 1. Topographic map showing location and magnitude of earthquakes that occurred on 26 December 2004 (M_w = 9.1) and 28 March 2005 (M_w = 8.6). Moment tensor solutions from the Harvard CMT catalog (http://www.seismology.harvard.edu/CMTsearch.html) are shown for main shocks on these days. CMT = Centroid Moment Tensor.

In the initial phase of generation of ESF irregularities, V_0 and V_C are highly variable due to the perturbation electric field associated with R-T plasma instability, which results in lower values of $C_l(x_0, t_m)$ (Bhattacharyya et al., 1989; 2001). But when this perturbation electric field is eroded, the ESF irregularities drift with the background plasma, resulting in less variability in V_0, V_c and values of $C_l(x_0, t_m)$ close to 1. It is found that on magnetically quiet days, after 22 LT the irregularities simply drift with the background plasma. Due to nonzero zenith angle of a signal path, vertical drift of irregularities V_z do contribute to V_0 and it is given by $V_0 = V_x - V_Z \tan\theta \sin A$, where θ is the zenith angle and A is the azimuth angle of the incoming signal measured eastward from north. The azimuth and zenith angle for the radio signal transmitted from geostationary satellite in the present case is 217° and 12.8°, respectively. As the contribution of V_z to V_0 is very small, the estimated V_0 represents the ambient zonal plasma drift, V_x. As we are exploring the earthquake-linked signatures in ionosphere over dip equatorial Indian station Tirunelveli, all figures are shown in Indian standard time (IST = UT + 5.5 hour).

3. Earthquake Details

Here we are studying two major earthquakes that occurred on 28 March 2005 and 26 December 2004 having magnitudes M_w = 8.6 and M_w = 9.1, respectively. The location of epicenter for these earthquakes are close to Sumatra, Indonesia, at 2.09°N, 97.15°E and 3.31°N, 95.85°E, respectively, which are marked in Figure 1. The earthquake that occurred on 26 December 2004 is the third largest earthquake recorded on seismograph, and it triggered a tsunami that caused tremendous large-scale natural diaster. The 2005 and 2004 earthquakes ruptured the boundary between the Indo-Australian plate, which moves generally northward at 40 to 50 mm/year, and the southeastern portion of the Eurasian plate, which is segmented into the Burma and Sunda subplates. These two earthquakes ruptured a 1,600-km-long portion of the fault boundary between the Indo-Australian and southeastern Eurasian plates on 28 March 2005 and 26 December 2004. The second event generated a tsunami that caused more than 283,000 deaths. The 2004 main shock rupture began at a depth of about 30 km at 00 hr:58 min:53 s UT (http://earthquake.usgs.gov), and the 2005 main shock rupture began at a depth of about 30 km at 16 hr:09 min:36 s UT. The focal mechanism solutions of the 2004 earthquake indicates predominantly thrust faulting on a shallowly (8°) dipping plane with a strike of 329°, whereas the 2005 earthquake was also predominantly dip-slip thrusting on a shallowly (7°) dipping plane with a strike of 329° (Ekström et al., 2005; Lay et al., 2005).

4. Results

Day-to-day variation in the occurrence of ESF irregularities and their characteristics and ambient *F* region parameters like electron density, electric field, conductivities, and height are well reported in many earlier studies (Burke et al., 2004; Gurram et al., 2018; Kakad, Tiwari, & Pant, 2012; Li et al., 2008; Nishioka et al., 2008; Yamazaki et al., 2018). Apart from day-to-day variations, these parameters are also affected by the modulated neutral winds resulting from the enhanced Joule energies at high latitudes and prompt penetration electric fields during periods of geomagnetic storms (Bhattacharyya et al., 2002; Kakad et al., 2011; 2017; Kikuchi et al., 2008). Thus, in order to identify and quantify the effects associated with earthquakes in the equatorial *F* region, it is important to verify the level of geomagnetic activity on the earthquake days. For this purpose, we checked variation of low-latitude and midlatitude geomagnetic activity indices, namely, *SYM-H*, a measure of ring current, and *Kp* for earthquake days. These indices are obtained from https://cdaweb.sci.gsfc.nasa.gov and plotted as a function of IST (UT + 5.5 hour) in Figure 2 for earthquake days including their respective preceding and following days. The top and bottom rows in Figure 2 show the variation of *SYM-H* and *Kp* indices for 27 – 29 March 2005 (Figures 2a and 2c) and 25 – 27 December 2004 (Figures 2b and 2d). Vertical black lines separate the earthquake day from the preceding and following days, whereas red dashed-dotted line indicates the start time of the earthquake for corresponding events. Generally, periods with $Kp > 3+$ are considered as geomagnetically active, which is shown by horizontal dotted lines in the bottom row. Most of the time during

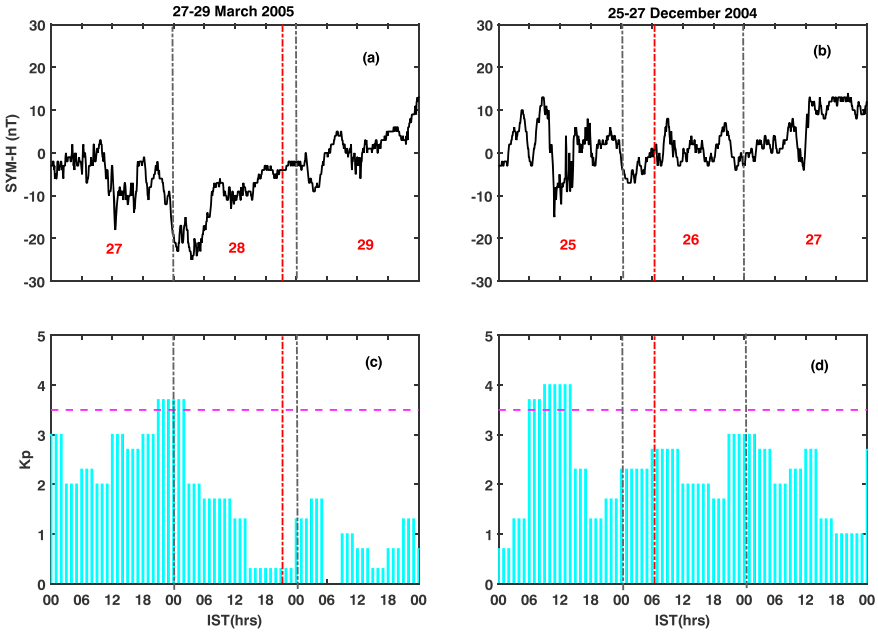

Figure 2. Low-latitude geomagnetic activity index *SYM-H* (top row) and midlatitude geomagnetic activity index *Kp* (bottom row) as a function of Indian standard time (IST = LT + 0.3 hr) for earthquake days (a, c) 28 March 2005 and (b, d) 26 December 2004. This plot includes the variation of these indices for 1 day preceding and 1 day following the earthquakes. The red dash-dotted lines indicate the start time of the earthquakes.

these 3-day periods the *Kp* index is below 4 and the *SYM-H* index is greater than −25 nT. It indicates that 3-day periods shown in Figure 2 are magnetically quiet. Thus, any unusual signatures manifested in the ionospheric *F* region observations beyond the quiet time day-to-day variability, on these two earthquake days, may be attributed to earthquake-linked mechanisms. In the following subsections we discuss the peculiar features observed during earthquake periods. Now onward we refer to the earthquakes that occurred on 28 March 2005 as event 1 and on 26 December 2004 as event 2.

4.1. Event 1: 28 March 2005

4.1.1. Effect on Zonal Plasma Drifts

In the post sunset hours usually the equatorial plasma bubbles (EPBs) are generated through RT plasma instability resulting in electron density irregularities of scale sizes extending from few centimeters to hundreds of kilometers. The presence of these ESF irregularities give rise to fluctuations in refractive index that impose phase perturbations on an incoming radio signal. Thus, when a radio signal passes through such irregular medium and propagates toward the ground, amplitude fluctuations are developed through phase mixing. Movement of the irregularities across the signal path causes spatial variations in the ground diffraction pattern to be converted into temporal fluctuations of the signal, which are called scintillations. As the electron density irregularities drift across the signal path, the scintillation pattern formed on the ground also drifts in the receiver's plane. Scintillations carry important information about the ESF irregularities. The irregularities of intermediate scale (100 m to few kilometers) contribute to scintillations on a Very High Frequency (VHF) signal. Generation of EPBs every day in the postsunset hour is not assured, and day-to-day variability in its occurrence is still an open question. Thus, the occurrence of amplitude scintillation every day in the postsunset hours is not guaranteed. So it is not possible to examine the continuous change (if any) in the ionospheric parameters few days before or after the earthquake. Rather, here we have considered all quiet days of the corresponding season to get the seasonal day-to-day variability and trends for the estimated parameters and compare these with their variation on the earthquake day. Such comparison helps to verify whether the effects observed on the earthquake day are well outside the day-to-day variability during that season or not. Also, the estimated seasonal averages of parameters will be statistically significant as they are derived from large number of observations.

As discussed in section 2, we estimated S_4, V_0, V_c, and $C_l(x_0, t_m)$ from spaced receiver scintillation observations. These parameters are shown as a function of IST for quiet days ($\sum Kp < 24$) of March–April 2005

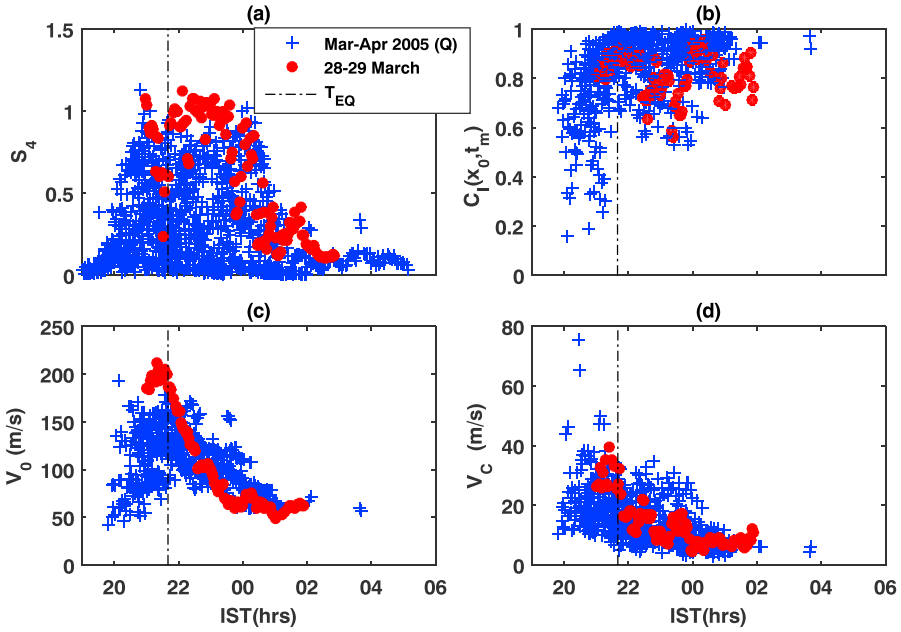

Figure 3. Variation of (a) S_4 index, a measure of strength of scintillation, (b) maximum cross correlation between two spaced receivers $C_l(x_0, t_m)$, (c) zonal irregularity drift V_0, and (d) random velocity V_c are plotted as a function of IST for quiet days of March–April 2005 (blue color) and earthquake day 28 March 2005 (red color). The time of start of earthquake T_{EQ} is shown by vertical dash-dotted lines in all subplots. IST = Indian standard time.

(i.e., vernal equinox in blue) and earthquake day 28 March 2005 (red) in Figure 3. The start time of earthquake (T_{EQ} = 21.7 IST hours) is marked by vertical dash-dotted line in respective subplots. Before we proceed to understand the earthquake-linked signatures manifested in these parameters, we will explain the quiet time seasonal patterns followed by these parameters and their physical meaning. In the post sunset hours, normally during the initial phase of development of ESF irregularities the parameter V_0 and V_c are highly variable and $C_l(x_0, t_m) \leq 0.5$ due to the presence of perturbation electric field associated with RT plasma instability. As the perturbation electric field can cause rapid change in the drift of ESF irregularities, the signals from two spaced receivers are found to be highly decorrelated producing lower values of maximum cross-correlation function (i.e., $C_l(x_0, t_m) < 0.5$). When the perturbation electric field associated with RT plasma instability is eroded, the ESF irregularities simply drift with the background plasma and the estimated V_0 represents the ambient zonal plasma drift. The random velocity V_c and $C_l(x_0, t_m)$ has a tendency to occupy lower and higher values, respectively, during this phase. It is evident in Figure 3 that the V_0, V_c, and $C_l(x_0, t_m)$ follow a well-defined pattern after 22 IST on magnetically quiet days (blue color). Before 22 LT the estimated irregularity drift V_o may have some contribution from the vertical irregularity drift V_Z.

S_4 index varies differently on each day depending on the space and time evolution of the ESF irregularities. On earthquake day 28 March 2005 (red color) clear difference in the zonal drift of ESF irregularities is noticed. The irregularity drift V_0 is found to be significantly higher than the quiet time values. This large zonal plasma drift is observed 20 min prior to the time of the earthquake. The maximum V_0 is approximately 212 m/s prior to earthquake at around 21.3 IST, whereas on quiet days the maximum V_0 is close to 150–160 m/s. This is an unusual feature because so far we have not noticed such a large enhancement in V_0 on either quiet or disturbed day (Engavale et al., 2006). Statistical study using long-term spaced receiver scintillation observations from the same station (Engavale et al., 2005) reported the average zonal drift of $\langle V_0 \rangle \approx 200$–$210$ m/s during the periods of high solar activity ($F_{10.7} > 180$) and $\langle V_0 \rangle \approx 90$–$100$ m/s during periods of low solar activity ($F_{10.7} < 100$). March 2005 and December 2004 both fall under the low solar activity period, having monthly average 10.7 cm solar flux of 96 and 100, respectively. Specifically, for event 1 and event 2 days the 10.7 cm solar flux values are 79 and 89, respectively. The climatological model proposed by Fejer et al. (2005) suggests the maximum zonal plasma drifts of 120–170 m/s in the postsunset hours over Jicamarca, where the geomagnetic field is weaker than Tirunelveli. Using optical technique, Mukherjee (2003) has reported the peak of zonal eastward

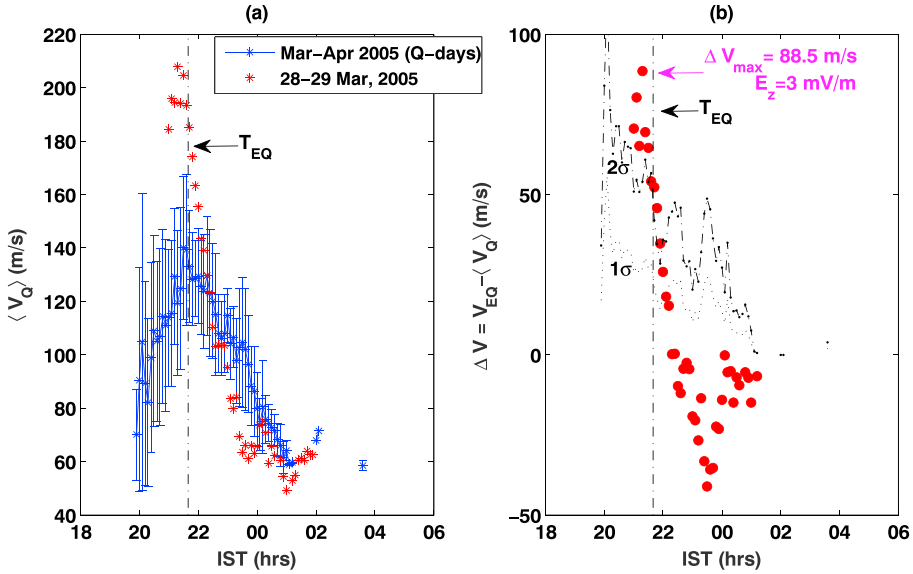

Figure 4. (a) Variation of average V_0 with error bars as a function of IST for quiet days of March–April 2005 (blue color) and earthquake day 28 March 2005 (red color). The standard deviation in $\langle V_0 \rangle$ is in the range of 3–41 m/s. (b) The difference in zonal irregularity drift on earthquake day as compared to their monthly quiet time variation is obtained by using $\Delta V = V_{EQ} - \langle V_Q \rangle$ and plotted as a function of IST. The dotted and dash-dotted lines respectively represent the 1σ and 2σ deviation in V_0 during quiet days. The time of start of earthquake T_{EQ} is shown by vertical dash-dotted lines in respective subplots. IST = Indian standard time.

drifts of 175 m/s during equinoctial months of solar maximum in the Indian sector. It implies that the observed enhanced zonal drift is indeed an unusual feature for low solar activity period like March 2005.

In order to quantify the effect on zonal plasma drifts, we estimated the averages of V_0 on quiet and earthquake days at every 6-min interval. Figure 4a shows quiet time average irregularities drift $\langle V_Q \rangle$, along with average zonal irregularity drift on earthquake day V_{EQ}. The difference between average zonal drifts on earthquake day and monthly quiet days is estimated ($\Delta V = V_{EQ} - \langle V_Q \rangle$) and plotted in Figure 4b. The start time of the earthquake is marked by vertical dotted lines in Figure 4. We found the maximum enhancement of 88.5 m/s in zonal plasma drift prior to the initiation of the earthquake. This enhancement is well above the quiet time day-to-day variability in the zonal plasma drifts for March–April 2005 as seen from the standard deviation plotted for each interval in Figure 4a. The standard deviation in average V_0 is in the range of $\sigma = 3$–41 m/s. The standard deviation in V_0 observed during quiet days is shown by the dotted line (1σ) and dash-dotted line (2σ) in Figure 4b to examine the statistical significance of observed deviation in zonal plasma drifts. In general, 2σ corresponds to the 95% confidence interval. It may be noted that the observed maximum deviation in zonal plasma drifts, that is, $\Delta V_{max} = 88.5$ m/s, is well beyond the 2σ. Thus, the observed deviation is 95% statistically significant.

Now we need to explore the possible sources responsible for the enhancement in zonal plasma drift. We know that in the equatorial latitudes the Earth's magnetic field is nearly horizontal, and in its presence the zonal neutral wind ($\vec{U}$) sets up the vertical electric field in the equatorial *F* region after sunset, through dynamo action such that $\vec{E}_z = -\vec{U} \times \vec{B}$, where *B* is ambient magnetic field and E_z is vertical electric field. So eastward neutral wind can set up the vertically downward electric field during the nighttime. This ambient vertically downward electric field (E_{z0}) causes ionospheric plasma to drift in the eastward direction with velocity $\vec{V}_x = -\vec{E_{z0}} \times \vec{B}/B^2$. It may be noted that in postsunset the ionospheric plasma drift with the neutral wind speed in the *F* region, when there is no other additional electric field of different origin (like geomagnetic activity or earthquake or perturbation electric field associated with RT plasma instability) to alter the ambient vertical electric field. First, the climatology of this season under low solar flux condition does not support the generation of such a large ambient vertically downward electric field. Second, as it is a quiet day, the possibility of presence of any additional electric field linked with geomagnetic activity in the low-latitude ionosphere is dismissed. It is to be noted from the plot of $C_I(x_0, t_m)$ for the earthquake day in Figure 3b that the irregularities that produced the scintillations had drifted onto the signal path from west side and the perturbation electric field

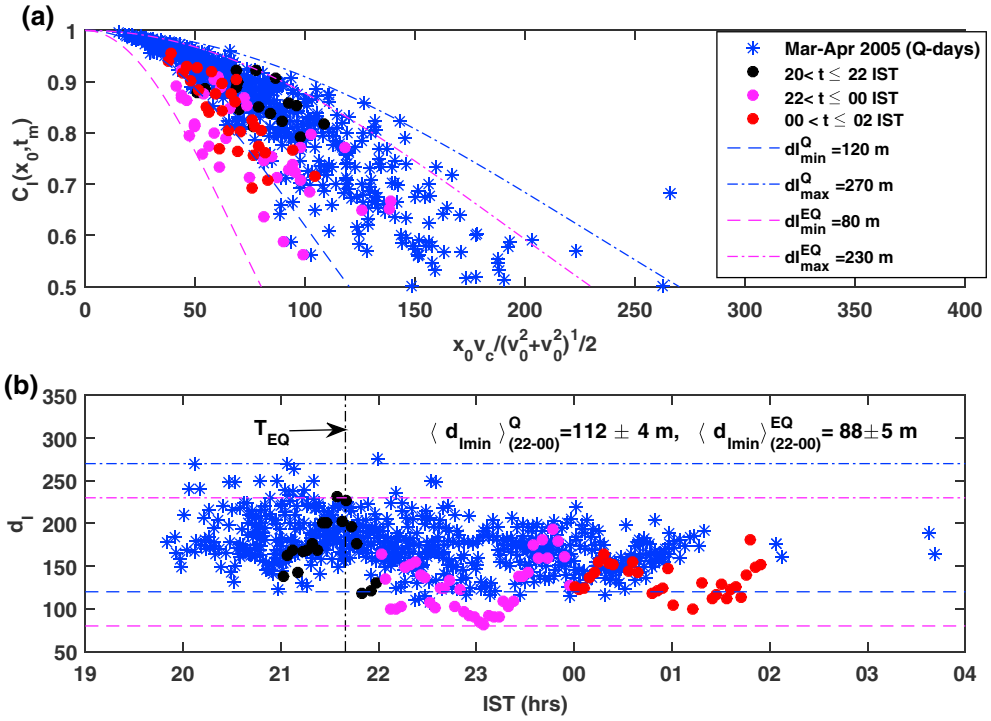

Figure 5. (a) Plot of $C_l(x_0, t_m)$ as a function of $x_0 V_c/(V_0^2 + V_c^2)^{1/2}$ for quiet days of March–April 2005 (blue color) and earthquake day 28 March 2005. This plot represents variation of spatial correlation function $C_l(x)$ as a function of x. (b) Coherence scale d_l as a function of IST for quiet days of March–April 2005 and earthquake day. The minimum and maximum coherence scale on quiet (earthquake) days are respectively marked by blue (magenta) dashed and dash-dotted lines in both panels. On quiet days coherence scales vary in the range of 120–270 m, and on earthquake day coherence scales vary in the range of 80–230 m. Time of earthquake is marked by vertical dash-dotted black line in the lower panel. The average lower bound of coherence scale $\langle d_{lmin} \rangle$ during 22-00 IST for quiet days and earthquake day are mentioned in lower panel. IST = Indian standard time.

associated with RT instability, which had generated these irregularities initially, had been nearly eroded. So only one possible source remains, and it is the earthquake-linked mechanism. The modulation of neutral winds due to the energy and momentum transferred to the *F* region through vertically propagating gravity waves resulting from earthquake will mostly contribute in the postseismic periods. Thus, the enhancement seen prior to the earthquake is likely to be linked with the electric field of seismic origin. As mentioned earlier, the zonal plasma drifts in *F* region are governed by $\vec{V}_x = -\vec{E}_{z0} \times \vec{B}/B^2$. IGRF model gives the ambient magnetic field of 34,178 nT at 300 km over Tirunelveli. Thus, the enhancement of 88.5 m/s in eastward drift would require an additional vertically downward electric field of 3 mV/m. The presence of such a strong vertically downward electric field in the equatorial *F* region prior to the earthquake at a location ≈ 2,200 km away from the epicenter of the earthquake is certainly an interesting feature.

The presence of vertical electric field close to the ground prior to the earthquake is reported in earlier studies. It is mainly attributed to the (i) emission of radioactive particle (radon) into the atmosphere within the area of seismic preparation zones (Pulinets & Boyarchuk, 2004) and (ii) activation of highly mobile positive holes (h^*) that carry charges during the rupture of stressed rocks (Freund, 2000; Freund et al., 2009). The radius R of the preparation zone is given by $10^{0.43M}$, where M is the earthquake magnitude (Dobrovolsky et al., 1979). For this event the dimension of preparatory zone comes out to be 4,988 km and the observation station is located well within the preparation zone (≈ 2,200 km away from the epicenter). A study by Kuo et al. (2011) has suggested that the stressed rock acts as a dynamo battery and supplies highly mobile charge carriers continuously to generate electric current, which maintains this additional vertical electric field on the ground. This current can be either vertically upward or downward directed. The magnitude of electric field present on the ground may be significantly higher (approximately few kilovolts), and it gets diminished (few millivolts) as we move toward the ionospheric altitudes. The mapping of earthquake-linked vertical electric field present at the lower boundary (85 km) of the ionosphere at the off-equatorial station to the equatorial *F* region and its

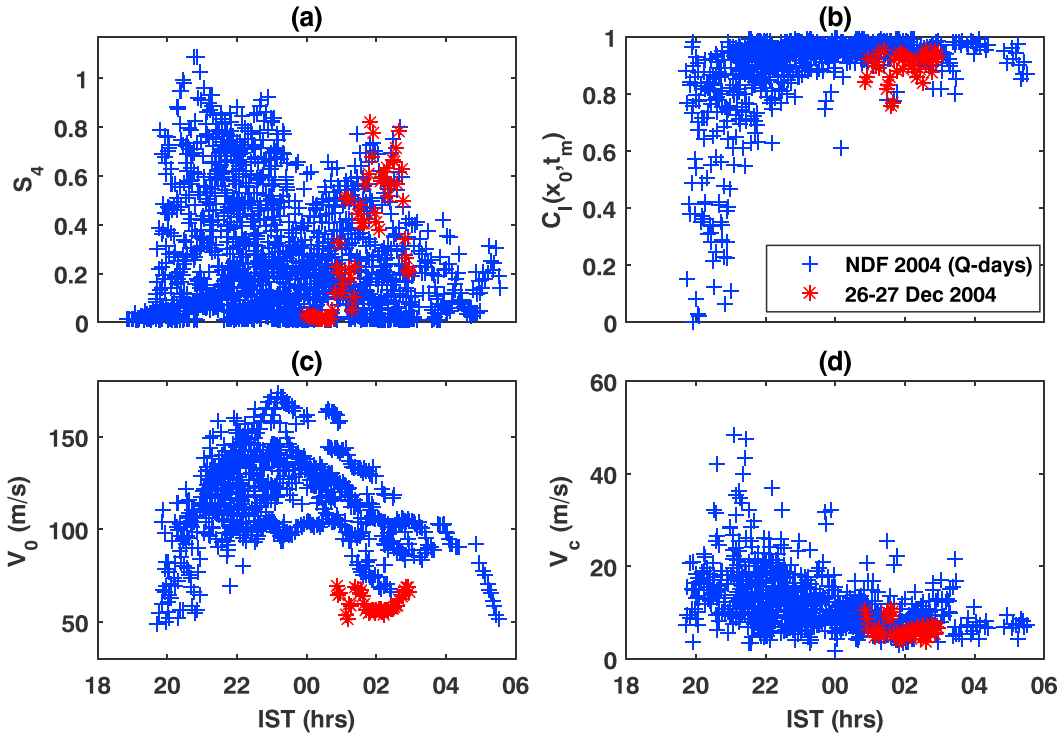

Figure 6. Variation of (a) S_4 index, (b) maximum cross correlation between two spaced receivers $C_l(x_0, t_m)$, (c) zonal irregularity drift V_0, and (d) random velocity V_c are plotted as a function of IST for quiet days of December solstice of 2004 (blue color) and postearthquake day 27 December 2004 (red color). Earthquake occurred on 26 December 2004 at 6.48 IST. December solstice includes November 2004, December 2004, and February 2005, which is termed as NDF. IST = Indian standard time.

influence on redistribution of electron density has been demonstrated through three-dimensional simulation (Kuo et al., 2014). The element radon is a radioactive element present in the gaseous form and has a half-life time of 3.8 days. Highly energetic particles like alpha and beta and electromagnetic radiation like gamma rays emitted during the radioactive disintegration of radon cause the ionization of neutral atmosphere over seismically active zone before an earthquake. Thus, it contributes positively to the increase of electrical conductivity of the atmosphere. During fair weather the magnitude of the downward vertical electric field present on the ground is found to be in the range of 100–200 V/m. However, during earthquake period (preseismic and coseismic) the magnitude of electric field can be enhanced significantly due to the presence of an additional electric field (Choudhury et al., 2013; Pulinets et al., 2006). Also, the direction of electric field can be either upward or downward. Kim et al. (1994) have calculated the penetrated electric field in the ionosphere to be about 1 mV/m, for a given external vertical electric field of 1 kV/m on the ground, by using a simple model with an upper boundary of 90 km. Although this model is developed for the midlatitude and high latitude, it demonstrates that the strong vertical electric field present on the ground can penetrate till ionospheric altitudes. By using a dense array of continuously monitoring GPS stations, Heki (2011) found ionospheric electron enhancements 40 min before the 2011 Tohoku-Oki earthquake (M_w= 9.1) in Japan. The ionospheric electron enhancements were initiated 25–80 min before earthquakes of magnitude 8 or 9 (Heki & Enomoto, 2015).

4.1.2. Spatial Scales of ESF Irregularities

We also looked into the variation of coherence scale d_l on earthquake day and quiet days of corresponding month using a method introduced by Bhattacharyya et al. (2003). This method is valid for both weak and strong scintillations, unlike power spectral analysis, which is valid only for weak scintillations (Kakad, Nayak, & Bhattacharyya, 2012; Yeh & Liu, 1982). Coherence scale is the scale at which spatial correlation function falls to half of its maximum value of unity at ground, that is, $C_l(x = d_l, 0) = 0.5$. It gives information about the dominant spatial scale present in the ground scintillation pattern. $C_l(x)$ as a function of x is obtained by plotting $C_l(x_0, t_m)$ as a function of $x_0 V_c/(V_0^2 + V_c^2)^{1/2}$. Figure 5a shows the distribution of coherence scale for quiet days of March–April 2005 (blue color) and earthquake day 28 March 2005 at different times. Let us assume $C_l(x)$ as Gaussian function having the form $\exp(-x^2/l_0^2)$. Using each value of $C_l(x_0, t_m)$ and corresponding value

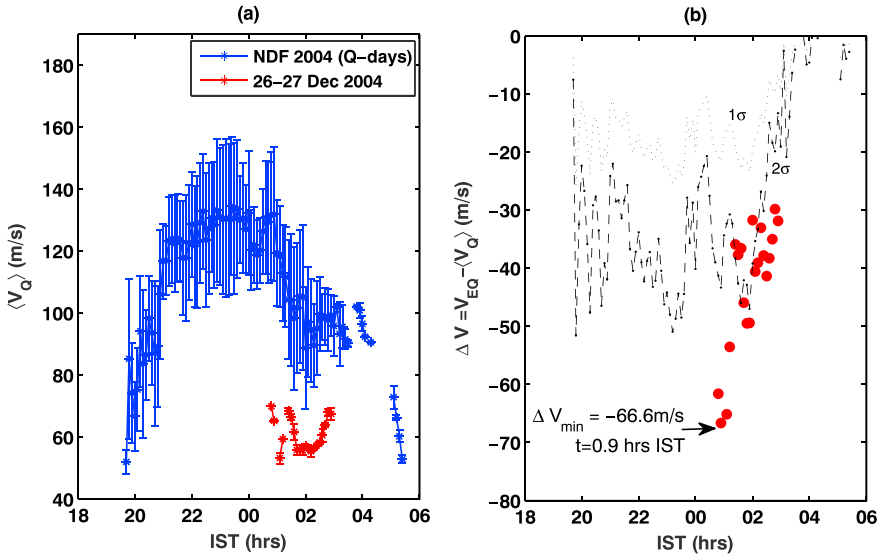

Figure 7. (a) Variation of average V_0 with error bars as a function of IST for quiet days of December solstice of 2004 (blue color) and postearthquake day, 27 December 2004 (red color). The standard deviation in $\langle V_0 \rangle$ is in the range of $\sigma = 7-25$ m/s. (b) The difference in zonal irregularity drift on postearthquake day, 27 December 2004 as compared to their seasonal quiet time variation is obtained by using $\Delta V = V_{EQ} - \langle V_Q \rangle$ and plotted as a function of IST. The dotted and dash-dotted lines represent the -1σ and -2σ deviation in V_0 during quiet days. The observed deviation in zonal plasma drift is statistically significant, and it is attributed to the earthquake- and tsunami-linked energy and momentum transferred to neutral atmosphere. NDF represents November 2004, December 2004 and February 2005. IST = Indian standard time.

of $x_0 V_c/(V_0^2 + V_c^2)^{1/2}$, we have computed l_0 by assuming the Gaussian-type spatial correlation function such that $l_0 = x_0 V_c/[\ln(1/C_l(x_0, t_m)) \times (V_0^2 + V_c^2)]^{1/2}$. Then we estimated the coherence scale as $d_l = 0.8326 l_0$. The variation of estimated coherence scale as a function of IST is depicted in Figure 5b.

It is noticed that on earthquake day the distribution of coherence scale is distinctly different as compared to other quiet days of March 2005. The spatial scales are very small at 80–230 m on earthquake day, whereas the spatial scales are found to be 120–270 m for all quiet days of March–April 2005. The minimum dl_{min} and maximum dl_{max} spatial scales observed on quiet (earthquake) day are shown by blue (magenta) dashed and dash-dotted lines, respectively, in Figure 5. These small-scale intermediate-scale irregularities are seen after the start of the earthquake around 22–00 IST, and they are associated with the strong scintillations ($S_4 = 0.9-1$). We computed the average value for the lower bound of coherence scale by taking the average of five minimum values of d_l for earthquake day and for March–April 2005. These values are specifically computed to get the lower bound of the coherence scale for earthquake day and quiet days of that season. The estimated average lower bound $\langle d_{l\min} \rangle$ during 22–00 IST for quiet days of March–April 2005 is 112 ± 4 m, whereas for earthquake day, 28 March 2005, it is 88 ± 5 m. The average lower bound in the spatial scales on earthquake day is well outside the regime of smaller coherence scale observed on quiet days of March–April 2005. In addition, we also computed the mean coherence scale during 22–02 IST for quiet period and earthquake day and it comes out to be $\langle d_l \rangle^{Q}_{(22-02)} = 168 \pm 25$ and $\langle d_l \rangle^{EQ}_{(22-02)} = 130 \pm 26$ m. The average coherence scale is found to be smaller for earthquake day. If we take $\pm 1\sigma$ deviations in their distributions, which is equivalent to 68.5% confidence interval, then their comparison suggests that the coherence scale for quiet and earthquake days lies in the range of 143–193 and 104–156 m, respectively. A slight overlap occurs in the range of coherence scales for these two distributions. So we can say that the observed lower coherence scales on earthquake day are nearly 68% statistically significant.

If we compare these results with theoretical model computations by Bhattacharyya and Yeh (1988) and Engavale and Bhattacharyya (2005), we understand that the (i) power spectrum for intermediate-scale ESF irregularities and (ii) density perturbation in the *F* region both play an important role in controlling the distribution of coherence scales in the ground scintillation pattern. The smaller coherence scales are produced through intermediate-scale ESF irregularities with shallower power spectrum $m = 2$ or $m = 3$. Also, d_l is inversely proportional to phase perturbations σ_ϕ, that is, higher phase perturbations support the

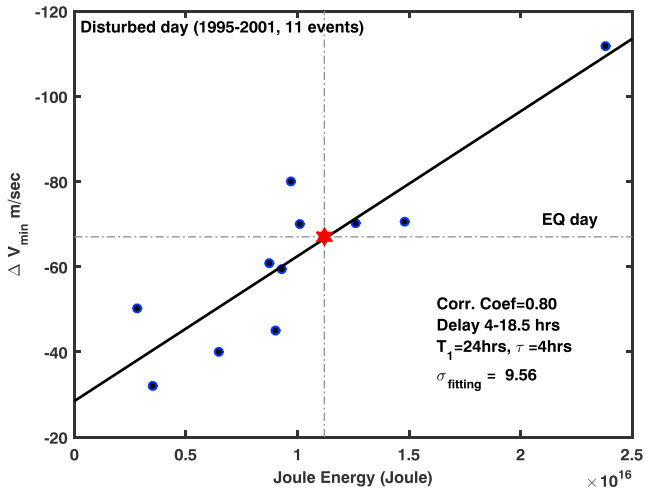

Figure 8. This plot is reproduced using information from Engavale et al. (2006). It shows plot of minimum deviation observed in zonal plasma drift on 11 magnetically disturbed days that occurred during 1995–2001 as a function of total Joule energy deposited in the high latitudes 4–18.5 hr before the local midnight. The red star represents the deviation of −66.6 m/s observed on the postearthquake day 27 December 2004. This deviation in zonal plasma drift is attributed to the earthquake- and tsunami-linked energy and momentum transferred to neutral atmosphere.

smaller spatial scales, when scintillations are strong. Thus, the smaller coherence scales associated with strong scintillations observed on earthquake day can be attributed to the presence of ESF irregularity with shallower power spectrum and strong density perturbation. The earthquake-linked electric field affects the structuring of EPBs and results into relatively small-scale ESF irregularities.

4.2. Event 2: 26 December 2004

4.2.1. The Effect on Zonal Drift

On 26 December 2004, an earthquake occurred in the morning time at 6.48 IST. During this time no scintillations were encountered as usually by 05–06 local time electron density irregularities associated with ESF get eroded due to increasing conductivities in the *E* regions connected to the equatorial *F* region through geomagnetic field lines. However, we have seen scintillations on 27 December in the early morning hours at 00–04 IST (IST = LT_{TIR} + 0.3 hour). Figure 6 shows the time variation of S_4, V_0, V_c, and $C_l(x_0, t_m)$ on 27 December 2004 (i.e., postearthquake night) with their variations on quiet days of December solstice (November 2004, December 2004, and February 2005) in background (blue color). It can be seen that zonal plasma drifts are relatively lower on 27 December 2004 as compared to their monthly quiet time variation of V_0. The signals from both receivers are found to be well correlated, and maximum cross correlation $C_l(x_0, t_m)$ is above 0.7. Also, random velocity V_C has lower values. It suggests that these ESF irregularities are not locally generated and drifted in from some other location situated toward the west side of the observation station. As the EPBs have drifted into the path of the signal, the perturbation electric field associated with RT plasma instability is considerably eroded. Hence, the ESF irregularity drift speed is not changing significantly due to the presence of such weak perturbation electric field associated with RT instability while drifting from west receiver to east receiver. In order to quantify the change in zonal plasma drift, we estimated 6-min average for quiet days of December solstice and 27 December 2004, which is shown in Figure 7a. The standard deviation in average V_0 is in the range of σ = 7–25 m/s. The difference between average zonal drifts on postearthquake night and quiet days of that season ($\Delta V = V_{EQ} - \langle V_Q \rangle$) is plotted in Figure 7b. The minimum deviation of −66.6 m/s at 0.9 IST hours is noticed. We plotted the standard deviation in V_0 observed on quiet days in Figure 7b to confirm the statistical significance of the observed deviation in V_0 on earthquake day. Here dotted and dash-dotted lines represent the -1σ and -2σ deviation in V_0. It may be noted that 2σ corresponds to the 95% confidence interval and the observed minimum deviation in zonal plasma drifts, that is, $\Delta V_{min} = -66.6$ m/s is outside the 2σ variation. Thus, the observed deviation is 95% statistically significant. Now negative deviation in V_0 at a given time implies that the zonal plasma drifts on postearthquake night was considerably smaller as compared to their monthly quiet time zonal plasma drifts. A notable feature is the effects on zonal plasma drifts that are seen nearly 18.5 hr after the time of arrival of main shock at epicenter for this earthquake. This is attributed to the neutral wind modulation caused in the lower and upper atmosphere due to the tsunami-linked energies. We find that the earthquake- and tsunami-linked effects persist in the equatorial *F* region nearly 2,200 km away from the epicenter of the earthquake even after 18.5 hr.

Such decrease in *F* region zonal plasma drift is a common feature seen on magnetically disturbed days, and it is attributed to the long-term and short-term disturbance dynamo (DD) effects operative during magnetically disturbed days (Blanc & Richmond, 1980; Scherliess & Fejer, 1997). Earlier studies have demonstrated that eastward zonal plasma drifts are not only diminished but sometimes reverse to westward (Fejer & Scherliess, 1997; Kakad et al., 2016; Ma & Maruyama, 2006). This DD is set up through enhanced heating of neutrals at high latitudes due to increased conductivities and currents, referred to as Joule heating. It activates neutral wind propagation from high to low latitudes. The mechanisms for short-term and long-term DD effects are obviously different. For the short-term effects the neutral wind disturbances do not have to reach the equator to alter equatorial electric field. The electric field and currents set up by the disturbance wind away from the equator, alter the equatorial electric field through current continuity (Fuller-Rowell et al., 2002). That is why short-term effects show up within a few hours. Compositional changes that cause the long-term effects need

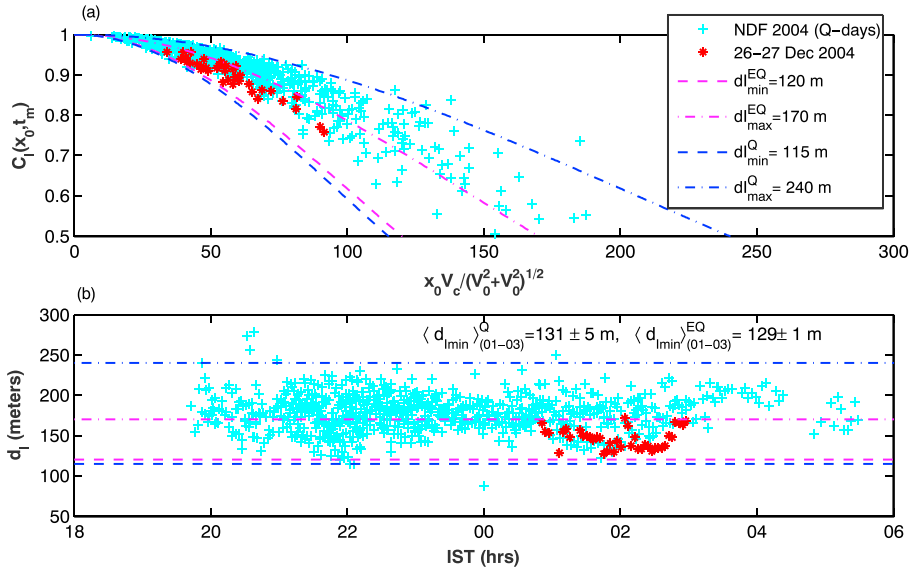

Figure 9. (a) Plot of $C_l(x_0, t_m)$ as a function of $x_0 V_c/(V_0^2 + V_c^2)^{1/2}$ for quiet days of December solstice of 2004 (cyan color) and 27 December 2004, postearthquake day (red color). This plot represents variation of spatial correlation function $C_l(x)$ as a function of x. (b) Coherence scale d_l as a function of IST for quiet days of December 2004 and postearthquake day. The coherence scales on quiet and postearthquake days are in the same range of 120–170 m during 00–04 IST. The average lower bound of coherence scale $\langle d_{lmin} \rangle$ during 01-03 IST for quiet days and earthquake day are mentioned in lower panel. NDF represents November 2004, December 2004 and February 2005. IST = Indian standard time.

to reach the equator and hence take much longer time. During its propagation the neutral wind experiences westward deflection due to Coriolis force in the middle to low latitudes in the Northern Hemisphere (Abdu, 2012), finally resulting in a westward plasma drift at low latitudes. The observed lower zonal drifts in the hours following an earthquake that triggered a tsunami is connected to the neutral wind modulation caused by earthquake- and tsunami-linked energy/momentum getting transferred to *F* region plasma through neutrals.

To get an idea about the energy required to produce a deviation of 66.6 m/s in zonal plasma drift, if it were caused by Joule heating during a magnetically disturbed period, we took information from our earlier work (Engavale et al., 2006). In this work, we have compared minimum deviation in ΔV on magnetically disturbed day and compared it with Joule energy deposited at high latitudes. The power associated with Joule heating is computed using the following equation (Akasofu, 1981):

$$P_{\text{Joule,Akasofu}} = 2 \times AE \times 10^8 W \tag{2}$$

Here *AE* is a high-latitude auroral electrojet index having sampling time of 1 min. The minimum deviation in zonal plasma drifts was mostly seen around local midnight, that is, T_m=00 LT hours. Different start time T_1 and end time $T_2 = T_m - \tau$ (here $\tau = 0, 2, ...15$ and $T_1 = 3, 9, ..27$ hr) were taken, and Joule energy is computed by integrating Joule power given by equation (2). The correlation between Joule energy and ΔV_{min} is compared for different time lags for 11 magnetically disturbed days occurring during 1995–2001. In that study we found that the minimum deviation in *F* region zonal drifts shows the minimum error in the least squares linear fit with the Joule energies deposited at high latitudes 4–18.5 hr before the local midnight (i.e., T_1 =24 and τ =4; see Figure 4 of Engavale et al., 2006). This particular combination of T_1 = 24 and τ = 4 results into highest correlation of r =0.8 between ΔV_{min} and Joule energy. These time lags are in general agreement with Fejer et al. (2005), which suggests that the *F* region zonal disturbance drifts over Jicamarca can be largely accounted for DD electric fields with dominant time delay of about 3–15 hr. We utilized this information from Engavale et al. (2006) and plotted ΔV_{min} as a function of Joule energy deposited 4–18.5 hr earlier in Figure 8. To produce maximum deviation of −66.6 m/s in *F* region plasma drifts on magnetically disturbed day, one requires Joule energy of 1.1×10^{16} J, which is marked with a red star in Figure 8. Thus, to see the maximum deviation of −66.6 m/s in *F* region zonal plasma drifts, which is observed nearly 18.5 hr after the initiation of an earthquake on 26 December 2004 that triggered a tsunami, on magnetically disturbed day energy of 1.1×10^{16} J would have to be deposited at high latitudes during 4–18 hr of magnetic activity prior to the time of observed effect.

It may be noted that the energy transfer processes involved in (i) energy transfer from high-latitude to low-latitude ionosphere through modulated neutral winds due to enhanced Joule heating at high latitudes on geomagnetically disturbed days and (ii) energy and momentum transferred to ionosphere from surface of Earth over earthquake preparation zone during and postearthquake/tsunami periods are different. These processes involve different spatial scales and time durations. The first scenario is commonly observed in the *F* region on disturbed days, whereas the second scenario is not so common and it is observationally limited due to occurrence frequency of major earthquakes. On 26 December 2004, the effect of earthquake/tsunami-linked energy and momentum transferred to the ionosphere is clearly evident in the *F* region zonal plasma drift, and it persists even 18.5 hr after the earthquake. Although these two processes are driven by different source mechanisms, both result in decrease in *F* region zonal plasma drifts by altering the ambient neutral winds. By comparing these two scenarios, we are not claiming that the source processes responsible for the observed deviation in *F* region zonal plasma drifts are same.

4.2.2. Spatial Scales of ESF Irregularities

We examined the coherence scale d_l associated with drift in EPBs observed in the postearthquake period, that is, on 27 December 2004 around 00–04 IST. Computation of coherence scale is elaborated in section 4.1.2. Figure 9a shows the $C_l(x_0, t_m)$ as a function of $x_0 V_c/(V_0^2+V_c^2)^{1/2}$ for quiet days of that season and for 27 December 2004. It represent the spatial correlation function $C_l(x)$, whereas Figure 9b gives variation of coherence scale d_l as a function of IST for quiet days of December solstice 2004 and for 27 December 2004. It is noticed that on 27 December 2004 the distribution of coherence scale is the same as that on other quiet days of the corresponding season. The spatial scales are varying in the range of 120–170 m for both 27 December 2004 and other quiet days of that season during 00–04 IST. We do not find any considerable difference in the structuring of the drift in EPBs on 27 December 2004.

5. Discussion

The source for preseismic ionospheric perturbation reported here for event 1 is not localized at the epicenter; in fact we have observed the earthquake-linked effects at approximately 2,200 km away from the epicenter. The earthquake-linked effects can be seen anywhere within the region of earthquake preparation zone, which has epicenter as its center. The area of the preparation zone varies with the magnitude of the earthquake, and it is calculated from the relation $R = 10^{0.43M}$, where R is the radius of earthquake preparation zone (in kms) and M is the earthquake magnitude (Dobrovolsky et al., 1979). For the first earthquake studied here, that is, 28 March 2005, the dimension of preparatory zone comes out to be 4,988 km. There are other studies that report the earthquake-linked signatures sufficiently far away from the epicenter. The Tohoku-Oki, Japan, earthquake ($M_w = 9.1$, epicenter: 38.32°N, 142.36°E), which occurred on 11 March 2011, triggered a tsunami, and the effect of this earthquake on vertical total electron content (VTEC) distribution was seen over a wider latitudinal (22°–45°N) and longitudinal belt (128°–150°E; ; Galvan et al., 2012). The VTEC in the region of 7°–16° (8°–14°) away from the epicenter in the latitudinal (longitudinal) direction was found to be influenced by earthquake activity, which covers nearly 1,800 km. Priyadarshi et al. (2011) have reported the anomalous increase and decrease in ionospheric total electron content few days prior to the earthquakes ($M_w > 5.0$) occurring within 2,000 km from the observation station. Recently, Chum et al. (2016) have reported the ionospheric signatures far outside the epicentral region (≈ 3,700–6,300 km from the epicenter) for the Nepal earthquake, which occurred on 25 April 2015. It is attributed to the ionospheric disturbances caused by long-period (20 s) infrasound waves that were excited by vertical displacement of ground, and they propagate vertically toward the ionosphere.

Here we find that the enhanced zonal plasma drift seen 20 min prior to the earthquake on 28 March 2005 indicates the presence of additional vertically downward electric field of magnitude 3 mV/m. Theoretical computation by Kim et al. (1994; 2012) indicates that the efficiency of the penetration of vertical electric field is larger during night due to lower ambient electrical conductivity as compared to day, and it strongly depends on the spatial extent and strength of the localized vertical electric field close to epicenter. In their theoretical calculations they have taken the upper boundary to be 90 and 170 km and assumed a Gaussian distribution for the electric field source on the ground. Their theoretical calculations indicate the presence of vertical electric fields of magnitude 0.3–0.7 mV/m at ionospheric altitudes for a large-scale (>100 km) seismic origin vertical electric field of magnitude 1,000 V/m on the ground. Although these theoretical estimates are given for midlatitudes and high latitudes, it demonstrates the penetration of seismic origin vertical electrostatic field to ionospheric altitudes, which is efficient during nighttime. For event 2 the deviation in zonal plasma

drifts is observed even after 18.5 hours. It is an evidence that the energy and momentum transferred to the *F* region through neutral wind modulation resulting from the acoustic waves generated during and after the earthquake/tsunami persist for longer time. During an earthquake, atmospheric pressure waves are generated due to a sudden impulsive forcing from the ground and they propagate upward into the atmosphere and ionosphere (generally in the form of gravity wave), which can result in decrease in the ambient plasma density at ionospheric altitudes (Astafyeva et al., 2013). Few studies have reported that the electron density in the ionosphere is perturbed by the atmospheric waves generated during an earthquake (Davies & Baker, 1965; Pulinets & Davidenko, 2014; Pulinets & Ouzounov, 2011).

6. Summary and Conclusions

It is important to identify and report the preseismic, coseismic, and postseismic signatures manifested in different observations in the near-Earth environment to improve our understanding of different mechanisms linked with earthquakes and their energy coupling to the lower and upper atmosphere. In the present study, we are reporting the equatorial ionospheric *F* region observations at dip equatorial station Tirunelveli in Indian longitude during two major earthquakes that occurred on 28 March 2005 ($M_w = 8.6$) and 26 December 2004 ($M_w = 9.1$). Both earthquakes had epicenter near Sumatra, Indonesia. We have used amplitude scintillation observations on a 251-MHz signal transmitted by geostationary satellite and recorded at Tirunelveli by two spaced receivers aligned in magnetic east-west direction. This observation station is radially nearly 2,200 km away from the epicenter of these two earthquakes. On 28 March 2005, we noticed large enhancement ($\approx$ 88.5 m/s) in the *F* region zonal plasma drifts as compared to their seasonal quiet time average of drifts 20 min prior to the start of the earthquake. This is an unusual observation because so far, even in the long-term scintillation observations recorded at Tirunelveli, we have not observed such enhancement in zonal plasma drift on a magnetically quiet or disturbed day (Engavale et al., 2006; Kakad et al., 2016; 2017). It implies the presence of additional vertically downward electric field of approximately 3 mV/m, which is linked with the earthquake. The scales of electron density irregularities of intermediate size (100 m to few kilometers) associated with ESF is found to be smaller as compared to their quiet time estimates. It implies that the earthquake-linked electric fields influenced the structuring and evolution of ESF irregularities as well. For the other earthquake (26 December 2004) the main shock arrived at around 6.48 IST and it triggered the tsunami. We have noticed that the tsunami-linked effects in the *F* region plasma drifts are distinctly manifested even 18.5 hr after the earthquake. The overall deviation in zonal plasma drift was found to be ≈ -66.6 m/s.

The effects on zonal plasma drifts for both earthquakes discussed in the present study are very distinct, and the mechanisms responsible for these two effects are entirely different. The effects observed on 28 March 2005 are linked with seismic origin electric fields, whereas the effects observed on 26 December 2004 are associated with neutral wind disturbances triggered due to extensive energies/momentum (mainly in the form of mechanical waves) transferred from the ground to neutral atmosphere during postearthquake and tsunami. The work carried out in the present study reports the important observational features of ionospheric *F* region that are crucial for better understanding of lithosphere-ionosphere coupling during earthquakes.

Acknowledgments
We thank CDAWEB for geomagnetic activity indices and NGDC NOAA for solar flux data. We thank USGS for earthquake information. We would also like to thank K. Jeeva for their technical support to the VHF spaced receiver experiment. We thank D. S. Ramesh for his valuable suggestions on the manuscript. A. B. acknowledges the Indian National Science Academy for an INSA senior scientist position at IIG. The VHF scintillation data will be made available on www.iigm.res.in on request at ebharati@iigs.iigm.res.in.

References

Abdu, M. (2012). Equatorial spread F/plasma bubble irregularities under storm time disturbance electric fields. *Journal of Atmospheric and Solar-Terrestrial Physics*, *75*, 44–56.

Akasofu, S.-I. (1981). Energy coupling between the solar wind and the magnetosphere. *Space Science Reviews*, *28*(2), 121–190.

Astafyeva, E., Rolland, L. M., & Sladen, A. (2014). Strike-slip earthquakes can also be detected in the ionosphere. *Earth and Planetary Science Letters*, *405*, 180–193. https://doi.org/10.1016/j.epsl.2014.08.024

Astafyeva, E., Shalimov, S., Olshanskaya, E., & Lognonné, P. (2013). Ionospheric response to earthquakes of different magnitudes: Larger quakes perturb the ionosphere stronger and longer. *Geophysical Research Letters*, *40*, 1675–1681. https://doi.org/10.1002/grl.50398

Baker, D. M., & Davies, K. (1968). Waves in the ionosphere produced by nuclear explosions. *Journal of Geophysical Research*, *73*(1), 448–451.

Bhattacharya, S., Sarkar, S., Gwal, A., & Parrot, M. (2009). Electric and magnetic field perturbations recorded by Demeter satellite before seismic events of the 17th July 2006 *M* 7.7 earthquake in Indonesia. *Journal of Asian Earth Sciences*, *34*(5), 634–644. https://doi.org/10.1016/j.jseaes.2008.08.010

Bhattacharyya, A., Basu, S., Groves, K. M., Valladares, C. E., & Sheehan, R. (2001). Dynamics of equatorial F region irregularities from spaced receiver scintillation observations. *Geophysical Research Letters*, *28*(1), 119–122. https://doi.org/10.1029/2000GL012288

Bhattacharyya, A., Basu, S., Groves, K. M., Valladares, C. E., & Sheehan, R. (2002). Effect of magnetic activity on the dynamics of equatorial F region irregularities. *Journal of Geophysical Research*, *107*(A12), 1489. https://doi.org/10.1029/2002JA009644

Bhattacharyya, A., Franke, S., & Yeh, K. (1989). Characteristic velocity of equatorial F region irregularities determined from spaced receiver scintillation data. *Journal of Geophysical Research*, *94*(A9), 11,959–11,969.

Bhattacharyya, A., Groves, K., Basu, S., Kuenzler, H., Valladares, C., & Sheehan, R. (2003). L-band scintillation activity and space-time structure of low-latitude UHF scintillations. *Radio Science*, *38*(1), 1004. https://doi.org/10.1029/2002RS002711

Bhattacharyya, A., & Yeh, K. (1988). Intensity correlation function for waves of different frequencies propagating through a random medium. *Radio Science*, *23*(05), 791–808.

Blanc, M., & Richmond, A. (1980). The ionospheric disturbance dynamo. *Journal of Geophysical Research*, *85*(A4), 1669–1686. https://doi.org/10.1029/JA085iA04p01669

Briggs, B. H. (1984). The analysis of spaced sensor records by correlation techniques, *Middle atmosphere program, handbook for map* (Vol. 13, pp. 166–186). United States: International Council of Scientific Unions Middle Atmosphere Program.

Burke, W. J., Gentile, L. C., Huang, C. Y., Valladares, C. E., & Su, S. Y. (2004). Longitudinal variability of equatorial plasma bubbles observed by DMSP and ROCSAT-1. *Journal of Geophysical Research*, *109*, A12301. https://doi.org/10.1029/2004JA010583

Cahyadi, M. N., & Heki, K. (2013). Ionospheric disturbances of the 2007 Bengkulu and the 2005 Nias earthquakes, Sumatra, observed with a regional GPS network. *Journal of Geophysical Research: Space Physics*, *118*, 1777–1787. https://doi.org/10.1002/jgra.50208

Choudhury, A., Guha, A., De, B. K., & Roy, R. (2013). A statistical study on precursory effects of earthquakes observed through the atmospheric vertical electric field in northeast India. *Annals of Geophysics*, *56*(3), 0331.

Chum, J., Liu, J.-Y., Laštovička, J., Fišer, J., Mošna, Z., Baše, J., & Sun, Y.-Y. (2016). Ionospheric signatures of the April 25, 2015 Nepal earthquake and the relative role of compression and advection for Doppler sounding of infrasound in the ionosphere. *Earth, Planets and Space*, *68*(1), 24.

Currie, J., & Waters, C. (2014). On the use of geomagnetic indices and ULF waves for earthquake precursor signatures. *Journal of Geophysical Research: Space Physics*, *119*, 992–1003. https://doi.org/10.1002/2013JA019530

Dautermann, T., Calais, E., Haase, J., & Garrison, J. (2007). Investigation of ionospheric electron content variations before earthquakes in Southern California, 2003–2004. *Journal of Geophysical Research*, *112*, B02106. https://doi.org/10.1029/2006JB004447

Davies, K., & Baker, D. M. (1965). Ionospheric effects observed around the time of the Alaskan earthquake of March 28, 1964. *Journal of Geophysical Research*, *70*(9), 2251–2253. https://doi.org/10.1029/JZ070i009p02251

Depueva, A. (2012). Peculiarities of low-latitude and equatorial ionosphere prior to strong earthquakes. *Geomatics, Natural Hazards and Risk*, *3*(3), 207–224. https://doi.org/10.1080/19475705.2011.619206

Dieminger, W., & Kohl, H. (1962). Effects of nuclear explosions on the ionosphere. *Nature*, *193*(4819), 963.

Dobrovolsky, I., Zubkov, S., & Miachkin, V. (1979). Estimation of the size of earthquake preparation zones. *Pure and Applied Geophysics*, *117*(5), 1025–1044.

Doocy, S., Daniels, A., Packer, C., Dick, A., & Kirsch, T. D. (2013). The human impact of earthquakes: A historical review of events 1980–2009 and systematic literature review. *PLoS Currents*, *5*.

Ekström, G., Dziewoński, A., Maternovskaya, N., & Nettles, M. (2005). Global seismicity of 2003: Centroid–moment-tensor solutions for 1087 earthquakes. *Physics of the Earth and Planetary Interiors*, *148*(2-4), 327–351.

Engavale, B., & Bhattacharyya, A. (2005). Spatial correlation function of intensity variations in the ground scintillation pattern produced by equatorial spread-F irregularities. *Indian Institute of Geomagnetism*, *31*(1), 23–32.

Engavale, B., Jeeva, K., Nair, K. U., & Bhattacharyya, A. (2005). Solar flux dependence of coherence scales in scintillation patterns produced by ESF irregularities. *Annales Geophysicae*, *23*(10), 3261–3266. https://doi.org/10.5194/angeo-23-3261-2005

Engavale, B., Jeeva, K., Nair, K., & Bhattacharyya, A. (2006). Effect of magnetic activity on equatorial F region plasma drifts. In *Proceedings of ILWS workshop* (pp. 432). India.

Fejer, B. G., & Scherliess, L. (1997). Empirical models of storm time equatorial zonal electric fields. *Journal of Geophysical Research*, *102*(A11), 24,047–24,056.

Fejer, B. G., Souza, J., Santos, A., & Costa Pereira, A. (2005). Climatology of F region zonal plasma drifts over Jicamarca. *Journal of Geophysical Research*, *110*, A12310. https://doi.org/10.1029/2005JA011324

Freund, F. (2000). Time-resolved study of charge generation and propagation in igneous rocks. *Journal of Geophysical Research*, *105*(B5), 11,001–11,019.

Freund, F. T., Kulahci, I. G., Cyr, G., Ling, J., Winnick, M., Tregloan-Reed, J., & Freund, M. M. (2009). Air ionization at rock surfaces and pre-earthquake signals. *Journal of Atmospheric and Solar-Terrestrial Physics*, *71*(17-18), 1824–1834.

Fuller-Rowell, T., Millward, G., Richmond, A., & Codrescu, M. (2002). Storm-time changes in the upper atmosphere at low latitudes. *Journal of Atmospheric and Solar-Terrestrial Physics*, *64*(12-14), 1383–1391.

Galvan, D. A., Komjathy, A., Hickey, M. P., Stephens, P., Snively, J., Tony Song, Y., et al. (2012). Ionospheric signatures of Tohoku-Oki tsunami of March 11, 2011: Model comparisons near the epicenter. *Radio Science*, *47*, RS4003. https://doi.org/10.1029/2012RS005023

Garcia, R., Crespon, F., Ducic, V., & Lognonn, P. (2005). Three-dimensional ionospheric tomography of post-seismic perturbations produced by the Denali earthquake from GPS data. *Geophysical Journal International*, *163*(3), 1049–1064. https://doi.org/10.1111/j.1365-246X.2005.02775.x

Garmash, S., Lin'kov, Y. M., Petrova, L., & Shved, G. (1989). Generation of atmospheric oscillations by seismic-gravity oscillations of the Earth. *Izvestiya, Atmospheric and Oceanic Physics*, *25*, 952–959.

Geller, R. J. (1997). Earthquake prediction: A critical review. *Geophysical Journal International*, *131*(3), 425–450.

Ghobarah, A., Saatcioglu, M., & Nistor, I. (2006). The impact of the 26 December 2004 earthquake and tsunami on structures and infrastructure. *Engineering Structures*, *28*(2), 312–326.

Gupta, S., & Upadhayaya, A. (2017). Pre-earthquake anomalous ionospheric signatures observed at low-mid latitude Indian station Delhi during the year 2015 to early 2016: Preliminary results. *Journal of Geophysical Research: Space Physics*, *122*, 8694–8719. https://doi.org/10.1002/2017JA024192

Gurram, P., Kakad, B., Bhattacharyya, A., & Pant, T. (2018). Evolution of freshly generated equatorial spread F (F-ESF) irregularities on quiet and disturbed days. *Journal of Geophysical Research: Space Physics*, *123*, 7710–7725. https://doi.org/10.1029/2018JA025705

Hadjicontis, V., & Mavromatou, C. (1996). Electric signals recorded during uniaxial compression of rock samples: Their possible correlation with preseismic electric signals. *International Journal of Rock Mechanics and Mining Sciences and Geomechanics Abstracts*, *33*(7), 308A.

Hao, J. (1988). The anomalous of atmospheric electric field at the ground level and earthquakes. *Acta Seismologica Sinica*, *10*, 207–211.

Harrison, R. G., Aplin, K., & Rycroft, M. (2010). Atmospheric electricity coupling between earthquake regions and the ionosphere. *Journal of Atmospheric and Solar-Terrestrial Physics*, *72*(5-6), 376–381.

Heki, K. (2011). Ionospheric electron enhancement preceding the 2011 Tohoku-Oki earthquake. *Geophysical Research Letters*, *38*, L17312. https://doi.org/10.1002/jgra.50118

Heki, K., & Enomoto, Y. (2013). Preseismic ionospheric electron enhancements revisited. *Journal of Geophysical Research: Space Physics*, *118*, 6618–6626. https://doi.org/10.1002/jgra.50578

Heki, K., & Enomoto, Y. (2015). M_w dependence of the preseismic ionospheric electron enhancements. *Journal of Geophysical Research: Space Physics*, *120*, 7006–7020. https://doi.org/10.1002/2015JA021353

Ishii, M., Shearer, P. M., Houston, H., & Vidale, J. E. (2005). Extent, duration and speed of the 2004 Sumatra–Andaman earthquake imaged by the Hi-Net array. *Nature*, *435*(7044), 933.

Jordan, T. H., & Jones, L. M. (2010). Operational earthquake forecasting: Some thoughts on why and how. *Seismological Research Letters*, *81*(4), 571–574.

Kakad, B., Gurram, P., Tripura Sundari, P. N. B., & Bhattacharyya, A. (2016). Structuring of intermediate scale equatorial spread F irregularities during intense geomagnetic storm of solar cycle 24. *Journal of Geophysical Research: Space Physics*, *121*, 7001–7012. https://doi.org/10.1002/2016JA022635

Kakad, B., Nayak, C. K., & Bhattacharyya, A. (2012). Power spectral characteristics of ESF irregularities during magnetically quiet and disturbed days. *Journal of Atmospheric and Solar-Terrestrial Physics*, *81–82*(0), 41–49. https://doi.org/10.1016/j.jastp.2012.04.008

Kakad, B., Surve, G., Tiwari, P., Yadav, V., & Bhattacharyya, A. (2017). Disturbance dynamo effects over low-latitude F region: A study by network of VHF spaced receivers. *Journal of Geophysical Research: Space Physics*, *122*, 5670–5686. https://doi.org/10.1002/2016JA023498

Kakad, B., Tiwari, D., & Pant, T. (2011). Study of disturbance dynamo effects at nighttime equatorial F region in Indian longitude. *Journal of Geophysical Research*, *116*, A12318. https://doi.org/10.1029/2011JA016626

Kakad, B., Tiwari, D., & Pant, T. (2012). Study of post sunset vertical plasma drift at equatorial F-region using long-term (1990–2003) ionosonde measurements in Indian longitude. *Journal of Atmospheric and Solar-Terrestrial Physics*, *80*, 239–246.

Kelley, M. C. (2009). *The Earth's ionosphere: Plasma physics and electrodynamics* (Vol. 96). San Diego, CA: Academic Press.

Kelley, M. C., Vickrey, J. F., Carlson, C. W., & Torbert, R. (1982). On the origin and spatial extent of high-latitude F region irregularities. *Journal of Geophysical Research*, *87*(A6), 4469–4475. https://doi.org/10.1029/JA087iA06p04469

Kikuchi, T., Hashimoto, K. K., & Nozaki, K. (2008). Penetration of magnetospheric electric fields to the equator during a geomagnetic storm. *Journal of Geophysical Research*, *113*, A06214. https://doi.org/10.1029/2007JA012628

Kim, V., Khegai, V., & Illich-Svitych, P. (1994). On one possible ionospheric precursor of earthquakes. *Izvestiia-Russia Academy of Sciences Physics of the Solid Earth*, *30*, 223–226.

Kim, V., Liu, J., & Hegai, V. (2012). Modeling the pre-earthquake electrostatic effect on the F region ionosphere. *Advances in Space Research*, *50*(11), 1524–1533.

Kim, V. H. V., & Nikiforova, L. (1997). A possible generation mechanism of acoustic-gravity waves in the ionosphere before strong earthquakes. *Journal of Earthquake Prediction Research*, *6*, 584–589.

Kuo, C. L., Huba, J. D., Joyce, G., & Lee, L. C. (2011). Ionosphere plasma bubbles and density variations induced by pre-earthquake rock currents and associated surface charges. *Journal of Geophysical Research*, *116*, A10317. https://doi.org/10.1029/2011JA016628

Kuo, C., Lee, L., & Huba, J. (2014). An improved coupling model for the lithosphere-atmosphere-ionosphere system. *Journal of Geophysical Research: Space Physics*, *119*, 3189–3205. https://doi.org/10.1002/2013JA019392

Lay, T., Kanamori, H., Ammon, C. J., Nettles, M., Ward, S. N., Aster, R. C., et al. (2005). The great Sumatra-Andaman earthquake of 26 December 2004. *Science*, *308*(5725), 1127–1133.

Li, G., Ning, B., Liu, L., Zhao, B., Yue, X., Su, S.-Y., & Venkatraman, S. (2008). Correlative study of plasma bubbles, evening equatorial ionization anomaly, and equatorial prereversal $E \times B$ drifts at solar maximum. *Radio Science*, *43*, RS4005. https://doi.org/10.1029/2007RS003760

Lin, C., Hsiao, C., Liu, J., & Liu, C. (2007). Longitudinal structure of the equatorial ionosphere: Time evolution of the four-peaked EIA structure. *Journal of Geophysical Research*, *112*, A12305. https://doi.org/10.1029/2007JA012455

Liu, J., Chen, Y., Pulinets, S., Tsai, Y., & Chuo, Y. (2000). Seismo-ionospheric signatures prior to M 6.0 Taiwan earthquakes. *Geophysical Research Letters*, *27*(19), 3113–3116.

Liu, J. Y., Chuo, Y. J., Shan, S. J., Tsai, Y. B., Chen, Y. I., Pulinets, S. A., & Yu, S. B. (2004). Pre-earthquake ionospheric anomalies registered by continuous GPS TEC measurements. *Annales Geophysicae*, *22*(5), 1585–1593. https://doi.org/10.5194/angeo-22-1585-2004

Ma, J. Z. (2016). Atmospheric layers in response to the propagation of gravity waves under nonisothermal, wind-shear, and dissipative conditions. *Journal of Marine Science and Engineering*, *4*(1), 25.

Ma, G., & Maruyama, T. (2006). A super bubble detected by dense GPS network at East Asian longitudes. *Geophysical Research Letters*, *33*, L21103. https://doi.org/10.1029/2006GL027512

Marchand, R., & Berthelier, J.-J. (2008). Simple model for post seismic ionospheric disturbances above an earthquake epicentre and along connecting magnetic field lines. *Natural Hazards and Earth System Sciences*, *8*(6), 1341–1347.

Mukherjee, G. (2003). Studies of equatorial F-region depletions and dynamics using multiple wavelength nightglow imaging. *Journal of Atmospheric and Solar-Terrestrial Physics*, *65*(3), 379–390. https://doi.org/10.1016/S1364-6826(02)00214-6

Nishioka, M., Saito, A., & Tsugawa, T. (2008). Occurrence characteristics of plasma bubble derived from global ground-based GPS receiver networks. *Journal of Geophysical Research*, *113*, A05301. https://doi.org/10.1029/2007JA012605

Occhipinti, G., Aden-Antoniow, F., Bablet, A., Molinie, J.-P., & Farges, T. (2018). Surface waves magnitude estimation from ionospheric signature of Rayleigh waves measured by Doppler sounder and OTH radar. *Scientific Reports*, *8*(1), 1555.

Ouzounov, D., Pulinets, S., Kafatos, M. C., & Taylor, P. (2018). Thermal radiation anomalies associated with major earthquakes, *Pre-earthquake processes: A multidisciplinary approach to earthquake prediction studies* (pp. 259–274). Washington, DC: American Geophysical Union.

Oyama, K.-I., Kakinami, Y., Liu, J.-Y., Kamogawa, M., & Kodama, T. (2008). Reduction of electron temperature in low-latitude ionosphere at 600 km before and after large earthquakes. *Journal of Geophysical Research*, *113*, A11317. https://doi.org/10.1029/2008JA013367

Priyadarshi, S., Kumar, S., & Singh, A. (2011). Changes in total electron content associated with earthquakes ($M > 5$) observed from GPS station, Varanasi, India. *Geomatics, Natural Hazards and Risk*, *2*(2), 123–139.

Pulinets, S. (1998). Strong earthquake prediction possibility with the help of topside sounding from satellites. *Advances in Space Research*, *21*(3), 455–458.

Pulinets, S. (2009). Physical mechanism of the vertical electric field generation over active tectonic faults. *Advances in Space Research*, *44*(6), 767–773.

Pulinets, S. (2012). Low-latitude atmosphere-ionosphere effects initiated by strong earthquakes preparation process. *International Journal of Geophysics*, *2012*, 131842.

Pulinets, S., Bisiacchi, G., Berlinski, J., Dunajecka, M., & Vega, A. (2006). First results of the new type of measurements of atmospheric electric field in Mexico. *Bol-e*, *2*(4).

Pulinets, S., & Boyarchuk, K. (2004). *Ionospheric precursors of earthquakes*. Berlin: Springer Science & Business Media.

Pulinets, S., & Davidenko, D. (2014). Ionospheric precursors of earthquakes and global electric circuit. *Advances in Space Research*, *53*(5), 709–723.

Pulinets, S., & Ouzounov, D. (2011). Lithosphere–atmosphere–ionosphere coupling (LAIC) model—An unified concept for earthquake precursors validation. *Journal of Asian Earth Sciences*, *41*(4), 371–382.

Reddy, C. (1989). The equatorial electrojet. *Pure and Applied Geophysics*, *131*, 485–508.

Reddy, C., Sunil, A., González, G., Shrivastava, M. N., & Moreno, M. (2015). Near-field co-seismic ionospheric response due to the northern Chile M_w 8.1 Pisagua earthquake on April 1, 2014 from GPS observations. *Journal of Atmospheric and Solar-Terrestrial Physics*, *134*, 1–8.

Rhoades, D. A., & Evison, F. F. (2005). Test of the EEPAS forecasting model on the Japan Earthquake Catalogue. *Pure and Applied Geophysics*, *162*(6-7), 1271–1290.

Rolland, L. M., Lognonné, P., Astafyeva, E., Kherani, E. A., Kobayashi, N., Mann, M., & Munekane, H. (2011). The resonant response of the ionosphere imaged after the 2011 off the Pacific coast of Tohoku earthquake. *Earth, Planets and Space*, *63*(7), 62.

Rozhnoi, A., Hayakawa, M., Solovieva, M., Hobara, Y., & Fedun, V. (2014). Ionospheric effects of the Mt. Kirishima volcanic eruption as seen from subionospheric VLF observations. *Journal of Atmospheric and Solar-Terrestrial Physics*, *107*, 54–59.

Scherliess, L., & Fejer, B. G. (1997). Storm time dependence of equatorial disturbance dynamo zonal electric fields. *Journal of Geophysical Research*, *102*(A11), 24,037–24,046.

Shalimov, S., & Gokhberg, M. (1998). Lithosphere–ionosphere coupling mechanism and its application to the earthquake in Iran on June 20, 1990. A review of ionospheric measurements and basic assumptions. *Physics of the Earth and Planetary Interiors*, *105*(3), 211–218.

Shults, K., Astafyeva, E., & Adourian, S. (2016). Ionospheric detection and localization of volcano eruptions on the example of the April 2015 Calbuco events. *Journal of Geophysical Research: Space Physics*, *121*, 10,303–10,315. https://doi.org/10.1002/2016JA023382

Silina, A., Liperovskaya, E., Liperovsky, V., & Meister, C.-V. (2001). Ionospheric phenomena before strong earthquakes. *Natural Hazards and Earth System Science*, *1*(3), 113–118.

Spatz, D., Franke, S., & Yeh, K. (1988). Analysis and interpretation of spaced receiver scintillation data recorded at an equatorial station. *Radio Science*, *23*(03), 347–361.

Valladares, C., Sheehan, R., Basu, S., Kuenzler, H., & Espinoza, J. (1996). The multi-instrumented studies of equatorial thermosphere aeronomy scintillation system: Climatology of zonal drifts. *Journal of Geophysical Research*, *101*(A12), 26,839–26,850.

Walker, K. T., Ishii, M., & Shearer, P. M. (2005). Rupture details of the 28 March 2005 Sumatra M_w 8.6 earthquake imaged with teleseismic P waves. *Geophysical Research Letters*, *32*, L24303. https://doi.org/10.1029/2005GL024395

Wyss, M. (1997). Cannot earthquakes be predicted? *Science*, *278*(5337), 487–490.

Yamazaki, Y., Stolle, C., Matzka, J., Liu, H., & Tao, C. (2018). Interannual variability of the daytime equatorial ionospheric electric field. *Journal of Geophysical Research: Space Physics*, *123*, 4241–4256. https://doi.org/10.1029/2017JA025165

Yeh, K. C., & Liu, C.-H. (1982). Radio wave scintillations in the ionosphere. *Proceedings of the IEEE*, *70*(4), 324–360.

Zhang, X., Shen, X., Parrot, M., Zeren, Z., Ouyang, X., Liu, J., et al. (2012). Phenomena of electrostatic perturbations before strong earthquakes (2005–2010) observed on Demeter. *Natural Hazards and Earth System Sciences*, *12*, 75–83.

Zhou, Y., Yang, J., Zhu, F., Su, F., Hu, L., & Zhai, W. (2017). Ionospheric disturbances associated with the 2015 M7.8 Nepal earthquake. *Geodesy and Geodynamics*, *8*(4), 221–228.